SEDIMENTOLOGY the journal of the International Association of Sedimentologists

Sedimentology (2021) doi: 10.1111/sed.12906

An experimental investigation of sediment kinematics and multi-scale propagation for laboratory bed-load dunes

ALESSIO RADICE
Department of Civil and Environmental Engineering (DICA), Politecnico di Milano, Piazza Leonardo da Vinci 32, Milano, 20133, Italy (E-mail: alessio.radice@polimi.it)

Associate Editor – Subhasish Dey

ABSTRACT

The dynamics of river bedforms is still not well understood and detailed experimental investigation may provide significant insight into the process mechanisms. In this study, results are presented for a laboratory experiment that returned long time series of sediment kinematics for bed-load dunes. The run was performed in a closed conduit but, in the light of prior literature, the results are also representative of dunes under open-channel flows. A flow rate of 1.4 times the threshold for sediment transport was used, and the experiment lasted long enough to measure the sediment kinematics for four full dunes. This enabled a stability of mean values to be obtained for the key properties; concentration of moving sediment, sediment velocity and sediment transport rate, that were measured over a Eulerian grid. At a measuring location, all the properties present an oscillation pattern that resembles the passage of the dunes, also including higher-frequency oscillations (due to the flow turbulence) superimposed onto the low-frequency ones related to the dunes. The time evolution of the sediment transport rate is more similar to that of the sediment concentration than to that of the sediment velocity, which varies comparatively less. A multi-scale propagation is demonstrated considering the propagation of the dunes, of the sediment grains, and of quick 'sediment gusts' triggered by the flow field. Taking advantage of a Taylor-like hypothesis, that is assumed to be valid as a first-order approximation, a mean temporal evolution of the sediment–kinematics properties is determined. Although limited to a single hydro-dynamic condition, and thus in need of further testing, the present results are of interest for a number of applications, including bedform analysis, live-bed scour processes, and quantification of sediment transport rates by measuring surrogate quantities.

Keywords Bed-load transport, celerity of propagation, dunes, mean sediment motion pattern, sediment concentration, sediment transport rate, sediment velocity, Taylor-like hypothesis.

INTRODUCTION

Bedforms are ubiquitous in natural and industrial flows, developing in a number of processes where loose sediment is transported by a fluid; examples include aeolian transport, subaqueous forms under unidirectional or oscillating free-surface flows, as well as flows of fluid/sediment mixtures in pipelines. In this manuscript, attention is focused onto dunes created by a unidirectional flow of water, like river dunes. The interest for this kind of form has been traditionally stimulated by relevant applications (transport of sediment and attached substances,

implications for the flow field over an oscillating boundary, bed roughness and hydro-dynamic resistance); comprehensive reviews of these applications have been provided, for example, by Engelund & Fredsøe (1982), Best (2005), Coleman & Nikora (2011) and Charru *et al.* (2013).

Coleman & Nikora (2011) reported that the formation of dunes from an initially planar bed had been attributed to instabilities of the flow/bed system (e.g. Engelund & Fredsøe, 1982), to the bursting structures of turbulent boundary layers (e.g. Jackson, 1976), or to granular transport mechanics. Therefore, Coleman & Nikora (2011) proposed a two-stage phenomenological description according to which eddy-transport events create small initial disturbances that later grow until reaching a stable size. Some debate still exists on the triggering factors of the initial disturbances, but the idea of a growth of the latter to developed bedforms is common. Furthermore, Engelund & Fredsøe (1982) argued that the mechanism responsible for the formation of bed waves could be the same for open-channel and closed-conduit flows. In this respect, Coleman *et al.* (2003) and Cardona Florez & De Moraes Franklin (2016) studied the formation and development of bed oscillations in closed conduits. Coleman *et al.* (2003) attributed the formation of initial wavelets to discontinuities in the bed, while the growth of the forms to some stable shape was attributed to sediment trapping by the wavelets and bedform coalescence.

Once developed, bedforms make the near-bed flow field differ from that over a flat sediment surface. The essential description of a two-dimensional flow field over a train of dunes (e.g. Best, 2005) involves flow detachment at the crest of a dune, a recirculation zone downstream of the crest, then flow reattachment and development of a boundary layer over the tail of a downstream dune. The process is then cyclically repeated as the boundary layer reaches the front of the next dune. Numerous studies have been performed to characterize the motion of the fluid or of suspended sediment above dunes (e.g. Nelson & Smith, 1989; Kadota & Nezu, 1999; Wilson & Hay, 2016; Unsworth *et al.*, 2018). As mentioned above, the local features of the flow field determine the head losses of the bulk flow. Furthermore, developed dunes migrate along a channel as a result of sediment mass conservation. Sediment is eroded from a dune tail and deposits in the recirculation region downstream of the next dune crest, thus determining dune propagation. These considerations have stimulated, during the past decades, extensive research on the features of bed-load dunes, mostly focused on their size (amplitude and length, which result in total roughness height) and temporal properties (period and celerity of migration, which are important propagation scales of the sediment transport process). Examples of contributions to this research field are those of Van Rijn (1984), Julien & Klaassen (1995), Kuhnle *et al.* (2006) and Venditti *et al.* (2016), among others.

The bulk properties of the bed-load dunes are obviously a result of local sediment transport, but the latter has received little attention in the past, presumably due to the inherent difficulty of measuring it. On the other hand, studies of the sediment mechanics over a flat bed have considerably benefited from detailed investigation of the sediment motion patterns, mostly by image-based measurement methods (recent examples include those of Lajeunesse *et al.*, 2010; Roseberry *et al.*, 2012; Radice *et al.*, 2013; Heays *et al.*, 2014; Fathel *et al.*, 2015; Heyman *et al.*, 2016; Fraccarollo & Hassan, 2019). Recently, Tsubaki *et al.* (2018) presented detailed measurements of sediment motion patterns over two-dimensional and three-dimensional bed-forms; Terwisscha van Scheltinga *et al.* (2018, 2019) also adopted a Eulerian approach and provided measurements of sediment velocity over the tail of bed-load dunes in a laboratory flume, in an attempt to: "bridge the gap between measurements of bedload transport at the particle-scale and at the bedform-scale". Ashley *et al.* (2020) instead took a Lagrangian approach to analyze the probability distributions of travel time and hop distances for bed-load particles over equilibrium mobile bedforms; Wenzel & De Moraes Franklin (2019), finally, presented results for particle tracking over a barchan dune, that is a different case since it involves migration and lowering of an isolated sediment heap over a smooth bed. However, measurements of the bed-load sediment motion over bed dunes are still extremely scarce, and frequently limited in space and time. For example, Tsubaki *et al.* (2018) presented results from 75 s acquisitions over a bed area of 10×20 cm^2 (reported as a scale for one dune) and with a frame rate of 120 frames per second (fps). The measurements of Terwisscha van Scheltinga *et al.* (2019) included several 10 s, 90 fps series acquired at intervals of some minutes over one dune with a length of approximately 0.7 m. By contrast, characteristic temporal scales of dunes (for example, a period) may be easily as large as

some hundred seconds in experimental installations; in addition, dune trains typically include an indefinite series of bedforms which are similar to one another but not always the same, calling for long experimental durations to be used in bedform observation and analysis.

This paper thus presents long time series of the sediment motion over bed-load dunes in a closed laboratory conduit that was also used by Radice (2019) to perform several experiments with a range of flow rates from 1.2 to 1.6 times a threshold value for sediment transport. In those earlier experiments, the bed elevation was measured at some locations along the conduit. For increasing discharge, the dunes: (i) were progressively higher (actually they were detected for a minimum flow rate of 1.3 times the threshold value, while they were not emerging by the lowest flow rate), with a trend of increase similar to that predicted by the equation of Van Rijn (1984), albeit with a factor of overestimation around 2; (ii) had lower period and autocorrelation length; (iii) migrated faster along the conduit; and (iv) had a wavelength apparently independent of the flow properties, as mentioned also in other works (Coleman *et al.*, 2003; Cardona Florez & De Moraes Franklin, 2016), and in satisfactory agreement with the predictor of Julien & Klaassen (1995). Frequency spectra of the bed elevation presented a scaling range with a slope of around −3, in agreement with a value reported by Coleman & Nikora (2011) and references therein. The present study is instead for a single experiment with a flow rate of 1.4 times the threshold one. Sediment kinematic properties (concentration of moving sediment, velocity and solid discharge) were measured over a Eulerian grid, for a relatively large area and a duration of 35 min that was long enough to get data for a sequence of four complete dunes. The experiment duration also enabled stable mean values to be obtained for the sediment kinematic properties. Based on the data analysis, the manuscript provides an answer to the following question: how are the sediment kinematic properties distributed in time and space over a train of dunes? The manuscript first presents the experiment and the methods used to measure the sediment kinematics. Experimental results are described and discussed in terms of: (i) a general phenomenology; (ii) a multiscale propagation of different features (the dunes, the bed-load sediment and 'sediment gusts' to be better defined later); and (iii) mean sediment motion patterns over a train of dunes. Finally, the impact of this study is argued and concluding remarks are provided.

MATERIALS AND METHODS

The experiment

The present experiment was performed at the Hydraulics Laboratory 'Fantoli' (LIF) of the Politecnico di Milano, Milan, Italy, using a rectangular, covered channel that is 5.8 m long, 0.4 m wide and 0.16 m high. A sediment layer of 3 cm was spread along the entire conduit, resulting in an average flow height of 0.13 m. Sediment material (a mixture of white and black particles) was uniform Polybutylene terephthalate (PBT) with a density of 1.27 kg m^{-3}, equivalent particle size (diameter of a sphere having the volume of one grain) of 3 mm, and aspect ratio of roughly 2 as the ratio of the longest axis to the shortest one (Campagnol *et al.*, 2015). The conduit is equipped with an electro-magnetic flow-meter to measure the discharge and an upstream sediment feeder to run experiments in equilibrium transport conditions. The feeder is based on the forward–backward motion of a slotted plate placed beneath a hopper; when the slot is beneath the hopper it gets filled and when it is pushed forward it releases sediment into the flume. The sediment feeding rate is adjusted, changing the slot size and period of forward–backward motion. The accuracy of the feeder for time-mean sediment rates was determined as around 1% by Campagnol *et al.* (2013).

The threshold flow rate for sediment transport and the feeder settings for a range of flow rates were established in preliminary runs of Radice & Lauva (2017) and Radice (2019). It is known that large uncertainties exist in the estimation of incipient-motion conditions for sediment (e.g. Buffington & Montgomery, 1997; Buffington, 1999); in order to cope with these, Radice & Lauva (2017) determined a threshold flow discharge ($Q_c = 13.2$ l s^{-1}) as that inducing a weak sediment transport rate, following a proposal of Schvidchenko & Pender (2000). The threshold dimensionless sediment transport rate per unit width was equal to 5.6×10^{-5} as proposed by Radice & Ballio (2008). Radice (2019) showed that this approach returned a sediment transport capacity curve that was valid for a variety of laboratory experiments (using sand or lightweight sediment, as well as open-channel or closed-conduit flows) with ratios of the flow rate to the

threshold value from 0.9 to 1.6, and dimensionless sediment transport rates for unit width $\Phi = Q_s/[B(g\Delta d^3)^{0.5}] = 6.8 \times 10^{-7}$ to 9.7×10^{-2} (Q_s = sediment transport rate; B = flume width; g = gravity acceleration; $\Delta = s - 1$ with s = ratio of sediment density to water density; d = particle size).

The experiment presented in this manuscript had a discharge to threshold ratio $Q/Q_c = 1.4$. This is in the middle of the range experienced by Radice (2019) and was a convenient compromise between obtaining well-developed dunes and maintaining a relatively low bed-load (to avoid hindering the measurement of the sediment motion with the image-based methods described below). The bed was initially scraped to make it flat and was sprayed with water to avoid particles being lifted by flowing water that would be supplied afterwards; the conduit was carefully filled with water until a depth of few centimetres; after checking that the bed had not been altered significantly by the water arrival, the lid was installed and the conduit was completely filled with water flowing at a discharge of a few litres per second; finally, the flow rate was then increased up to a desired value of 18.5 l s^{-1}, corresponding to 1.4 times the threshold value. During the run, frequent checks were made at the electro-magnetic flow-meter to ensure that stationary flow conditions were maintained. The sediment feeding rate per unit width was equal to 6.2×10^{-6} m^2 s^{-1}.

The bed elevation was not recorded during the present experiment, while it had been measured extensively in the runs of Radice (2019). Figure 1 presents a sample temporal evolution of the bed elevation (run 5 of Radice, 2019) at a measuring location 5 m downstream of the conduit inlet. The succession of the dunes is evident, as well as the possible alternation between trains of smaller dunes and others of larger ones. These dunes had an amplitude of 22 mm, corresponding to 0.17 times the average flow height, and a mean period from spectral analysis of around 750 s; furthermore, repeated runs of Radice (2019) demonstrated a good repeatability of these measurements. The plot of Fig. 1 actually reveals a weak tendency of the mean bed to lower, indicating that the sediment feeding rate was slightly below the transport capacity. However, over 14 000 s this lowering determined an increase of the water height of only around 3%.

The present study considers a movie of the sediment motion taken in 2015. The flume bed was captured from above, at a working section approximately 4.5 m from the flume inlet, using an action camera (GoPro Hero 4 Black Edition; San Mateo, CA, USA). Action cameras have a good resolution and give the possibility to record for a long time, the shortcoming being instead a limited control of the focus length. The focus was thus not tuned specifically, and the image analysis involved a pre-processing phase as mentioned later. The camera was shooting at 30 fps with an image resolution of 1920×1080 pixels. The movie comprehends a total of 63 720 frames for a total duration of 35 min.

Sediment–kinematics parameters and image-based measurements

The movie frames were first converted into grey-scale images. Then, image distortion due to a short lens was removed as described in the video article of Radice *et al.* (2017). In order to save disk space, images were then cropped excluding unnecessary portions (basically, only a full width of the conduit was preserved). A sample cropped image is depicted in Fig. 2A, while a short video is provided as File S1 (downsampled at 15 fps and with a lower resolution to reduce the file size).

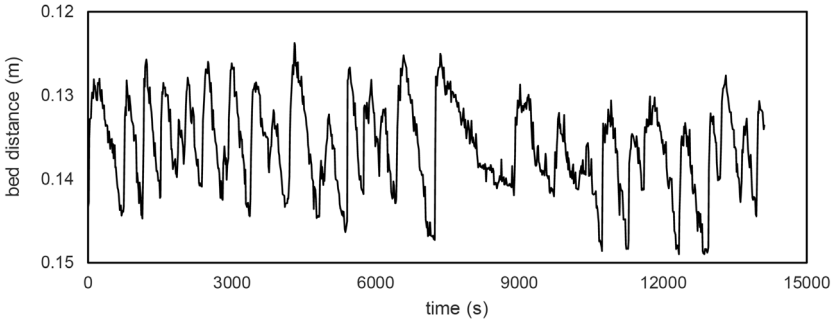

Fig. 1. Temporal evolution of the bed elevation in an experiment with $Q/Q_c = 1.4$ performed by Radice (2019). The ordinate axis is reversed as it represents a distance measured from the conduit lid to the bed.

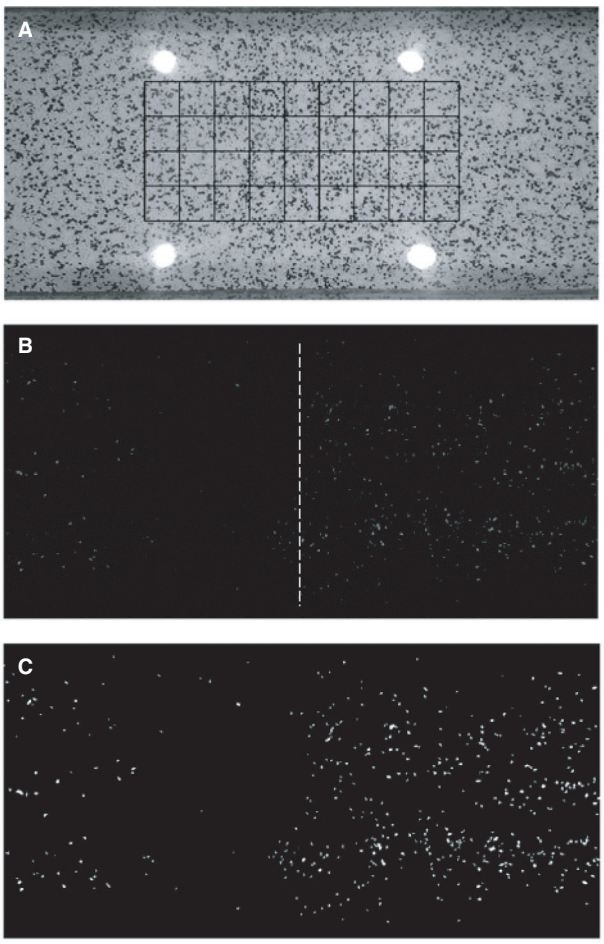

Fig. 2. (A) Sample image (flow is leftward) with the Eulerian grid used for the measurements (the square cells have a 5 cm side). (B) An image obtained by subtracting the frame in panel (A) from the following one in the experiment movie, with a dune front qualitatively sketched as the transition between intense sediment motion over the crest and negligible sediment motion in the recirculation zone. (C) Moving particles visualized by binarization and filtering, starting from the difference image.

Image analysis returned the measurement of the concentration and velocity of moving sediment, as well as the sediment transport rate per unit width computed as $q_s = C \times u \times d$ (C = concentration; u = sediment velocity). Here the term 'concentration' is used to quantify a relative mass of moving sediment; this parameter takes different names in the literature since, with appropriate factors, it can be converted into the 'activity' of, for example, Roseberry *et al.* (2012) or Heyman *et al.* (2016), or into the 'relative number of moving particles' defined by Ballio *et al.* (2018). In this study, the concentration is defined as $C = (N \times W)/(A \times d)$, with N as a number of particles moving over a measuring area A in the time interval that separates two successive frames, and W as the volume of one particle. Moving particles were identified by frame subtraction and filtering as depicted in Fig. 2B and C; in fact, frame subtraction reveals the moving particles but images obtained from differences contain a mixture of evident moving particles and noise, thus needing to be polished by suitable filtering that was performed through binarization and removal of the smallest white blobs after Radice *et al.* (2006). The velocity of the grains moving over A was measured by Particle Image Velocimetry (PIV) applied to pairs of difference images like that of Fig. 2B, again using the tools developed by Radice *et al.* (2006). The performance of image subtraction for recognition of moving particles is documented by File S2 that provides a short video built with image differences. All of the quantities were measured with a temporal interval of 1/30 s, equal to that used for image sampling. The measurement of the sediment concentration was calibrated in order to obtain a time-averaged value of the sediment transport rate per unit width equal to the sediment feeding rate supplied at the entrance of the conduit (a multiplicative constant was determined and applied to all the concentration measurements). It was shown before (Fig. 1) that the sediment feeding rate employed in this experiment had led to some bed lowering in an earlier test; one could then put into question an assumption of equality between the sediment feeding rate and the sediment transport rate at the working section. However, it was estimated that bed lowering could have determined changes of the sediment transport rate below 5%.

The measuring technique of Radice *et al.* (2006) is Eulerian, therefore a measuring grid is needed for individual values of the key properties to be attributed to single cells of the grid. In this work, square cells with a side of 5 cm were employed (thus $A = 25$ cm^2), as also depicted in Fig. 2A. Cells of 5 cm implied a smoothing of the dune fronts (that, based on direct observation during the experiment, was shorter than this length); however, this size was preferred to smaller ones, after some trials, to increase the reliability of the measurements and because, after all, it did not affect the measurements on the tails of the dunes where the properties obviously vary more smoothly than at the fronts.

The regions close to the lateral walls of the conduit were discarded to avoid possible wall effects, even if these were apparently negligible with dune fronts on average perpendicular to the flow direction (again see Files S1 and S2), and also to avoid the effect of the lamps used to illuminate the system (Fig. 2A). The grid extension was limited to the central part of the images due to degrading performance of the image correction in the outer regions. The total area of investigation thus spanned 45 cm and 20 cm in the stream-wise and transverse directions, respectively.

Terwisscha van Scheltinga *et al.* (2019) presented a comparison of sediment velocities obtained from PIV measurement to those from manual tracking of particles. Since any PIV algorithm attributes a velocity to a group of particles, they performed a regularization by averaging multiple velocity values from manual tracking before the comparison with one corresponding value from PIV. Also in the present study, a comparison is presented between sample velocity values measured manually and those measured by the PIV algorithm for the same image pairs (Fig. 3). Manually-obtained velocities have not been regularized by averaging, thus some bias is expected because the human eye is frequently caught by a most evident particle while the most probable displacement for a group of grains depends on all the moving particles in a measuring cell at a certain instant. Figure 3 reports the checks performed for a total of eight cells distributed within the measuring domain; for each cell, consecutive checks were separated by 1000 frames (see an example of the procedure in File S3). The point scatter in Fig. 3 is similar to that presented by Terwisscha van Scheltinga *et al.* (2019) and is considered satisfactory considering, moreover, that the manual values came from a single particle within any cell of the measuring grid.

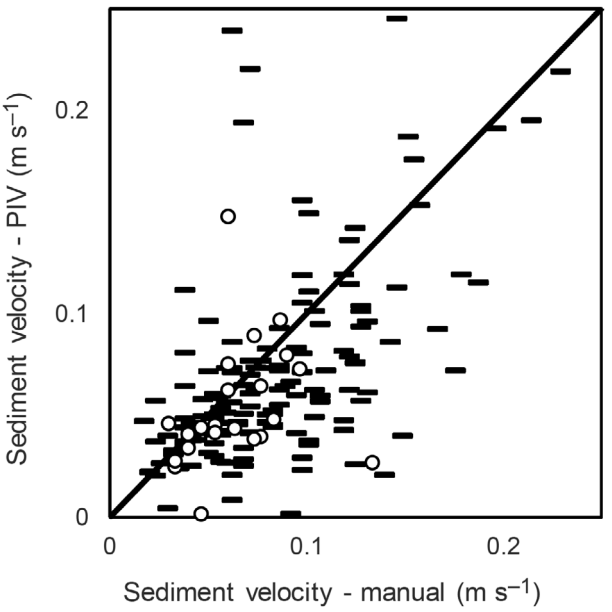

Fig. 3. Comparison of cell-based velocities measured by Particle Image Velocimetry (PIV) and velocities measured by hand on sample images. The white circles correspond to the checks made in File S3.

Sample temporal evolutions and convergence of mean values

The temporal signals measured at one sample location are depicted in Fig. 4, with plots presenting time evolutions for C, u and q_s. For all of the quantities, a 0.26 s and a 10 s moving average are shown; the former is representative of quasi-instantaneous behaviour while the latter was used to smooth the signals and obtain more regular patterns. Low-frequency and high-frequency fluctuations were present in all of the time evolutions. The temporal signal of C presented a shape similar to typical records of bed elevation at a fixed point, corresponding to the passage of successive dunes (for example, Fig. 1). Four full dunes were observed within the experiment duration. The dunes were not all the same, as one also obtains for measurements of bed elevation. The largest values of C were around 0.13, with a mean around 0.03. The temporal signal of sediment velocity also presented a succession of high and low values corresponding to the crests and troughs of the dunes, but the temporal evolution of u was flatter than that of C along the dune tails. Maximum and mean values were around 0.25 m s^{-1} and 0.06 m s^{-1} (versus a bulk flow velocity of 0.36 m s^{-1}). Finally, the time evolution of the sediment transport rate was a mixture of the two behaviours, more similar to that of C than to that of u. Maximum value of q_s was around 4×10^{-5} m^2 s^{-1} (more than six times the sediment feeding rate).

As mentioned above, the measurement of the concentration of moving sediment was calibrated in order to meet a prescribed value of the sediment transport rate per unit width (equal to the sediment feeding rate). Soundness of this approach requires a stable mean value of the sediment transport rate to be achieved at the end of

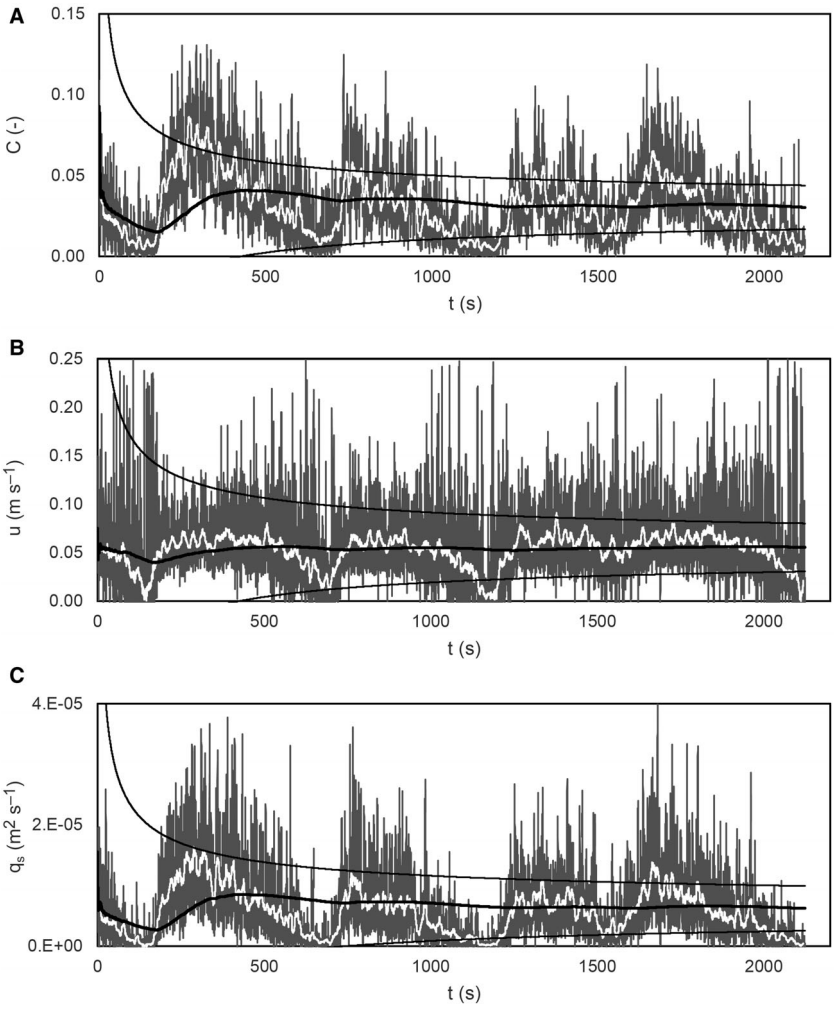

Fig. 4. Temporal signals for; (A) concentration of moving sediment, (B) velocity and (C) sediment transport rate at a sample location. Symbols: grey = 0.26 s moving average; white = 10 s moving average; black = progressive mean (thicker) and confidence limits.

the experiment duration. Therefore, Fig. 4 also includes a check of the convergence of the values computed by progressive means, where 95% confidence limits are computed as the final mean $\pm 2\sigma/(j/\mathrm{T})^{0.5}$ with σ as the standard deviation of a sample, j as a value counter and T as the integral scale of auto-correlation. The latter was set at 5400 values (corresponding to 180 s) following the quantification of Radice (2019) based on the records of bed elevation. This estimate was also checked by computing an auto-correlation function (not shown here) for a concentration signal that returned an integral scale of a bit more than 4000 values, then the estimation of Radice (2019) was preferred as being related to a longer measurement; however, this only impacts the amplitude of the confidence bands. The analysis of convergence shows that the line for the progressive mean was always within the confidence limits, this being actually caused by the large fluctuations that induced high values of the variances. The progressive means were reasonably flat in a last portion corresponding to the last two dunes. As remarked by Ballio & Guadagnini (2004), these analyses should be depicted using a logarithmic scale for the horizontal axis. Diagrams with a log axis are not shown here to save space and are included in File S4; however, the semi-log counterparts of the plots of Fig. 4 confirm the indication of a reasonable stability achieved in the last two dunes. This demonstrates that four dunes were enough to obtain stable values of the properties and, in turn, support the calibration of the concentration measurement based on the sediment feeding rate.

Estimation of propagation celerities

Since sediment transport is a propagation process, celerities were estimated for different

features (that are specified in a later section with experimental results) using cross-correlation analysis. Cross-correlation functions between two temporal signals f_1 and f_2 were computed as:

$$R(\tau) = \frac{\left(f_1'(t) \times f_2'(t+\tau) \right)_{av}}{\sigma_1 \sigma_2} \quad (1)$$

where R is a cross-correlation coefficient, τ is a temporal lag, σ_1 and σ_2 are the standard deviations of the two signals, a prime denotes a deviation from the mean value and a subscript '*av*' denotes averaging over all the possible pairs of products. A peak in a cross-correlation function enabled an associated temporal lag to be determined; the distance between the locations to which any f_1 and f_2 referred was divided by this lag to find a celerity of propagation.

RESULTS

Phenomenological description and interplay between the key quantities

The grains were sparsely entrained, transported for some distance, and then disentrained, as generally described for bed-load transport. Polar diagrams of sediment velocity (Fig. 5A) reveal the mainly one-dimensional nature of the particle motion. Some transverse motion was relatively more frequent in the troughs of the dunes, where the flow had detached from an upstream crest; in this wake region the sediment motion direction could also be opposite to that of the flow. Terwisscha van Scheltinga *et al.* (2019) also documented that transverse particle motion revealed the effect of the flow turbulence in the dune troughs. However, when a moving average over 10 s was considered, the particle motion appeared markedly one-dimensional. Furthermore, the transverse motion of sediment typically involved few particles, since the flux was depicted as strongly one-dimensional when a polar diagram of the sediment transport rate was produced (Fig. 5B).

It was mentioned above that the temporal variability of the sediment transport rate was similar to that of the sediment concentration, while the temporal evolution of the sediment velocity was somehow flatter. This is also revealed by correlation plots between the three quantities (Fig. 6), that return a quasi-linear relationship between the sediment concentration and the transport rate, while the velocity tends to achieve some plateau. Looking in more detail, in fact, for concentration values larger than the average a slope of a linear relationship between concentration and sediment transport rate is slightly damped by a lack of a corresponding increase of the sediment velocity. The observations now made for dunes are in agreement with those from earlier investigations of the sediment transport over a plane bed that mentioned that, once entrained by the flow, bed-load sediment presents a velocity that does not depend much on the hydro-dynamics, and that the fluctuations of the sediment transport rate are more similar to those of sediment concentration than to those of velocity (e.g. Drake *et al.*, 1988; Frey *et al.*, 2003; Ancey *et al.*, 2008; Heyman *et al.*, 2016). Furthermore, the sediment concentration varies much more than the sediment velocity as the flow strength increases, and the mean values of the sediment transport rate then reflect those of concentration more than those of velocity (e.g. Radice & Ballio, 2008).

Propagation celerity of bed-load dunes

Figure 7A compares the temporal evolution of the bed-load concentration at two locations that

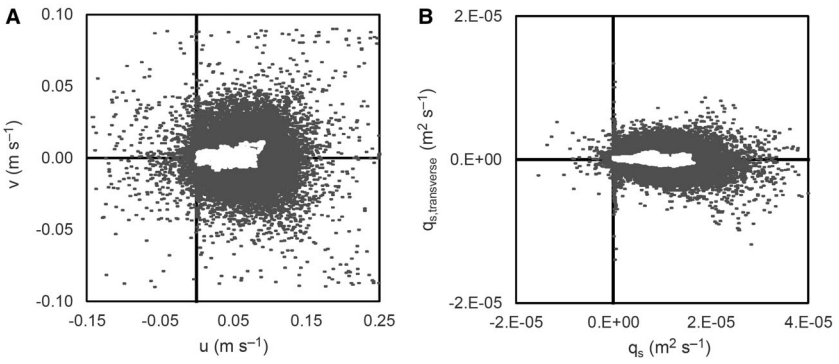

Fig. 5. (A) Polar plots of sediment velocity (with *v* as transverse component) and (B) of sediment transport rate per unit width. Symbols: grey = 0.26 s moving average; white = 10 s moving average.

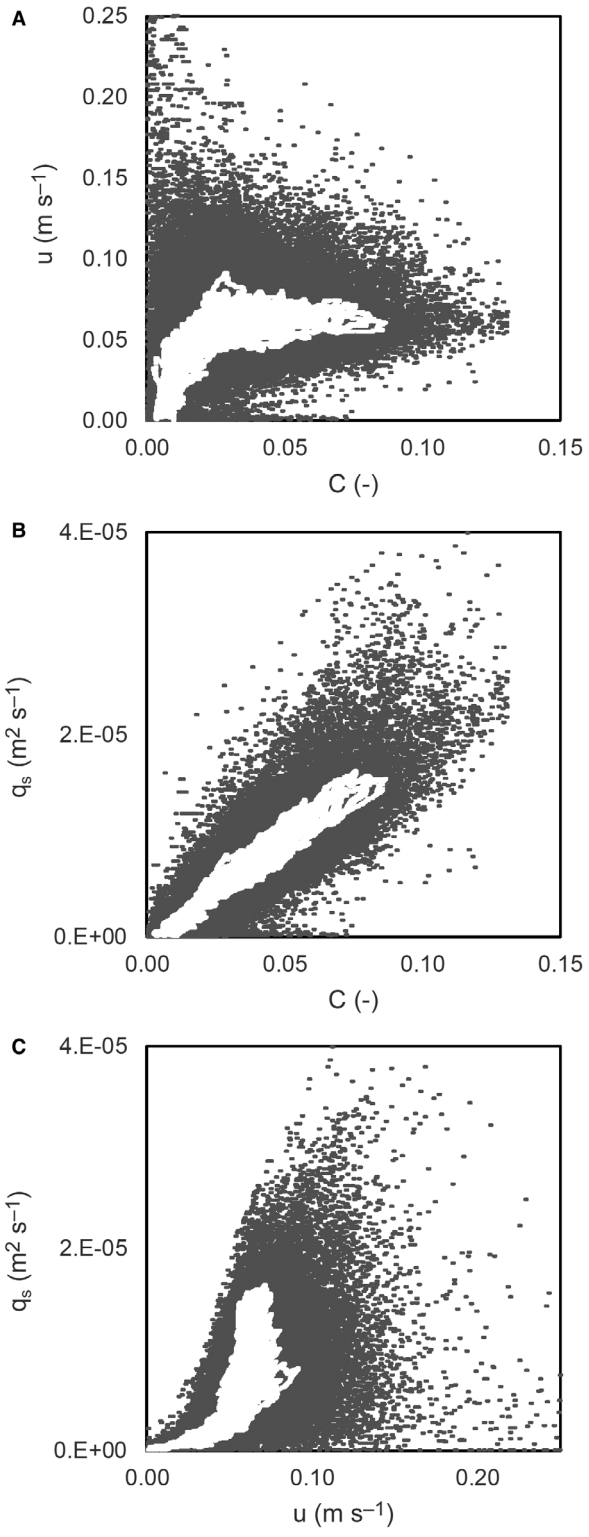

Fig. 6. Relationships between (A) sediment concentration and velocity, (B) sediment concentration and transport rate per unit width, and (C) sediment velocity and transport rate per unit width. Symbols: grey = 0.26 s moving average; white = 10 s moving average.

were 0.1 m apart along the stream-wise direction. These signals were obtained from a 20 s moving average to highlight the low-frequency fluctuations while damping the high-frequency ones. The two signals are evidently similar and temporally shifted, corresponding to the movement of the bed-load dunes from the upstream to the downstream location. Applying Eq. 1 to these two time evolutions, the cross-correlation function depicted in Fig. 7B is obtained. This function presents a highest peak for a time lag of 54.5 s, with a cross-correlation coefficient of 0.92. The τ value can then be converted into a celerity of propagation as described above, obtaining a celerity value of 0.0018 m s^{-1}.

The cross-correlation analysis was done for all the possible pairs of measuring locations with a 5 cm distance in the stream-wise direction; all the pairs for 10 cm and 15 cm distance were also considered to increase the size of an obtained sample of dune celerity values. The peak of the cross-correlation coefficient R was always quite high, ranging from 0.80 to 0.94 with a mean value of 0.89. Considering all the pairs of locations, an average value of the celerity of propagation for the bed-load dunes was obtained as equal to 0.0018 m s^{-1}, with a coefficient of variation (ratio of the standard deviation to the mean) of 0.08. The mean celerity value is in good agreement with that (0.0016 m s^{-1}) found by Radice (2019) for the same discharge by cross-correlating measurements of bed elevation at different points spaced by 1 m.

Propagation celerity of sediment gusts

In a bed-load process, quick and short-living gusts of sediment (collective motion of several particles) frequently appear, an observation dating back to Drake *et al.* (1988). Radice *et al.* (2009, 2010) applied the same image-based methods as used in this work and considered, for an experiment with weak bed-load transport over a plane bed, concentration signals at neighbouring cells. Furthermore, they employed cross-correlation analysis to quantify a propagation celerity of those signals where peaks were attributed to the mentioned sediment gusts. The latter were attributed to turbulent events displacing the sediment grains, and travelling at a celerity larger than both the particle velocity and a near-bed flow velocity (while being instead lower than the bulk velocity of the flow). Sediment gusts were observed also in the present case; the estimation of their propagation

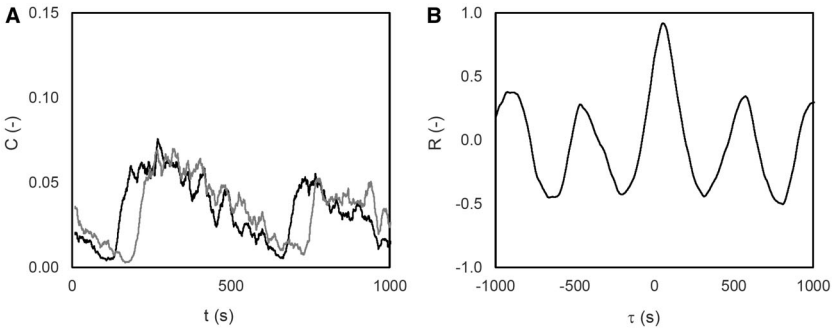

Fig. 7. (A) Concentration signals (20 s moving average) at two measurement locations spaced by 0.1 m (two-cell distance, upstream cell in black and downstream cell in grey). (B) Cross-correlation function obtained for these two signals. Panel (A) depicts only the first 1000 s while the cross-correlation was computed for the entire signal.

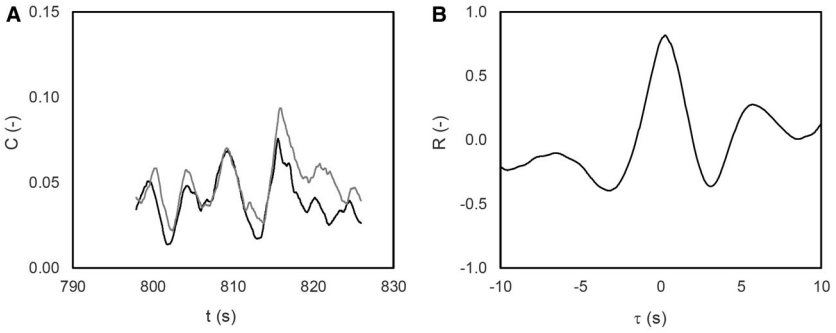

Fig. 8. (A) Concentration signals (2 s moving average) at two measurement locations spaced by 0.05 m (one-cell distance, upstream cell in black and downstream cell in grey). (B) Cross-correlation function obtained for these two signals.

celerity was determined applying the cross-correlation analysis to short-term portions of the concentration signals (because the cross-correlation for entire signals was always dominated by the migration of the dunes).

Figure 8A presents the temporal evolution of the concentration of moving sediment for two measuring locations that were 0.05 m apart along the stream-wise direction. Also in this case a moving average was applied to filter the effect of the highest frequencies, and these signals were obtained from a 2 s moving average. Applying Eq. 1 to these time evolutions returned the cross-correlation function depicted in Fig. 8 B, with a highest peak at a cross-correlation coefficient of 0.82 and determining a celerity value of 0.188 m s^{-1}. As done for the dunes, the cross-correlation analysis was repeated for all the possible pairs of measuring locations with a 5 cm distance along the stream-wise direction, to get a sample of celerity values. Furthermore, the estimation was done once for each of the four dunes (the example in Fig. 8 is for a 30 s portion of the second dune, as can be appreciated by looking at the time values compared to those of Fig. 3). The maximum value of R ranged from 0.46 to 0.91 with a mean value of 0.73. From all of the cross-correlation functions, an average value of the celerity of propagation for the sediment gusts was 0.185 m s^{-1}, with a coefficient of variation of 0.38. This celerity was thus higher than the sediment velocity and lower than the bulk flow velocity, as for the plane-bed cases reported above.

Mean sediment motion pattern over a train of dunes

Starting from the multiple realizations of temporal signals (one for each measurement location,

thus 36 realizations looking again at Fig. 2A), mean sediment motion patterns over dunes were computed. For the grid cells aligned by the transverse direction, the mean was synchronous; a similar operation could not be done for the grid cells aligned by the stream-wise direction, since the dunes migrated during the experiments and thus a delay was present from one signal to another (that delay was indeed the basis for estimating a celerity of propagation of the dunes as described above). Thus, the signals for the cells aligned by the stream-wise direction were averaged considering a temporal shifts multiple of 27.2 s, that is the time needed to travel 5 cm moving with a velocity of 0.0018 m s^{-1}. It was also shown above that the celerity of propagation of the sediment gusts, triggered by the flow turbulence, was two orders of magnitude larger than the celerity of the dunes, and larger than the particle velocity; thus, the averaging approach described above exploits a kind of Taylor-like hypothesis, assuming that the low-celerity features take a prominent role in propagating the transport. Briefly, the Taylor (1938) 'frozen-turbulence' hypothesis assumes that turbulent fluctuations do not significantly contribute to mass transport and, consequently, one can pass from the temporal to the spatial domain of investigation (and *vice versa*) considering the propagation velocity that characterizes the process. Figure 9 depicts the mean signals with a range of variation of one standard deviation (computed for each time over the sample of the realizations; symbols with a subscript 'm' indicate means over the realizations), and the temporal evolution of the coefficient of variation of the samples (again, one sample is made of the 36 values for a certain time). Actually, a 20 s moving average was applied to the signals before averaging over the realizations, to obtain a smoother trend and also for consistency with the averaging applied above to compute the celerity of the bed-load dunes. If the period of the preliminary moving average was reduced, the final signals would obviously be more fluctuating and the coefficient of variations for the realization samples would increase.

The plots of Fig. 9 show patterns similar to those obtained from the regularization of the signals for a single measuring cell (Fig. 4), again demonstrating the strong coherence of the dune patterns. The concentration of moving sediment is on average 3%, with a maximum value (with the 20 s regularization) of 7%. The plateaus for sediment velocity are around 0.07 m s^{-1}, around 20% of the bulk flow velocity; mean sediment velocity is 0.06 m s^{-1} (0.17 times the bulk flow velocity). Terwisscha van Scheltinga *et al.* (2019), here considered for comparison, measured mean velocities around 0.08 m s^{-1} with a bulk flow velocity of 0.5 m s^{-1} (with a similar ratio of 0.16). The coefficient of variation of the quantities (Fig. 9D) presents an opposite trend compared with those of the concentration, velocity and solid discharge; this is in agreement with earlier findings for sediment kinematics over a plane bed, for which more intense transport presents more regular statistics (e.g. Ancey *et al.*, 2008; Radice, 2009; Radice *et al.*, 2013).

The results presented so far answer the first part of the question posed in the *Introduction*, quantifying a temporal evolution of the sediment kinematic properties over the dunes. Moving further with the exploitation of a Taylor-like hypothesis, the temporal signals of Fig. 9 can be converted into spatial profiles, again considering the celerity of propagation of the dunes as a conversion factor. A dune profile over 3.5 m of length is obtained (not shown here but presented in File S4). The resulting dune length is equal to around 0.8 m; the latter is in agreement with the evaluations of Radice (2019) that started from measurements of the bed elevation at some points, and with the predictor of Julien & Klaassen (1995). Instead, the formula of Coleman *et al.* (2003) underestimated the length of these dunes, returning a dune length value of around 0.4 m.

DISCUSSION

Multi-scale propagation

The present results confirm a multi-scale propagation associated with the motion of bed-load dunes. Celerities were defined for the dunes themselves and for quick sediment gusts. The latter are reasonably induced by turbulent structures of the flow field, analogous to the eddy-transport events introduced by Coleman & Nikora (2011); furthermore, Terwisscha van Scheltinga *et al.* (2019) also recalled Furbish *et al.* (2017) who mentioned the turbulent events travelling and influencing the fluctuations of the sediment transport. In addition to these celerities, the sediment velocity is also an obvious scale of propagation. Figure 10 depicts the separation detected between these scales of

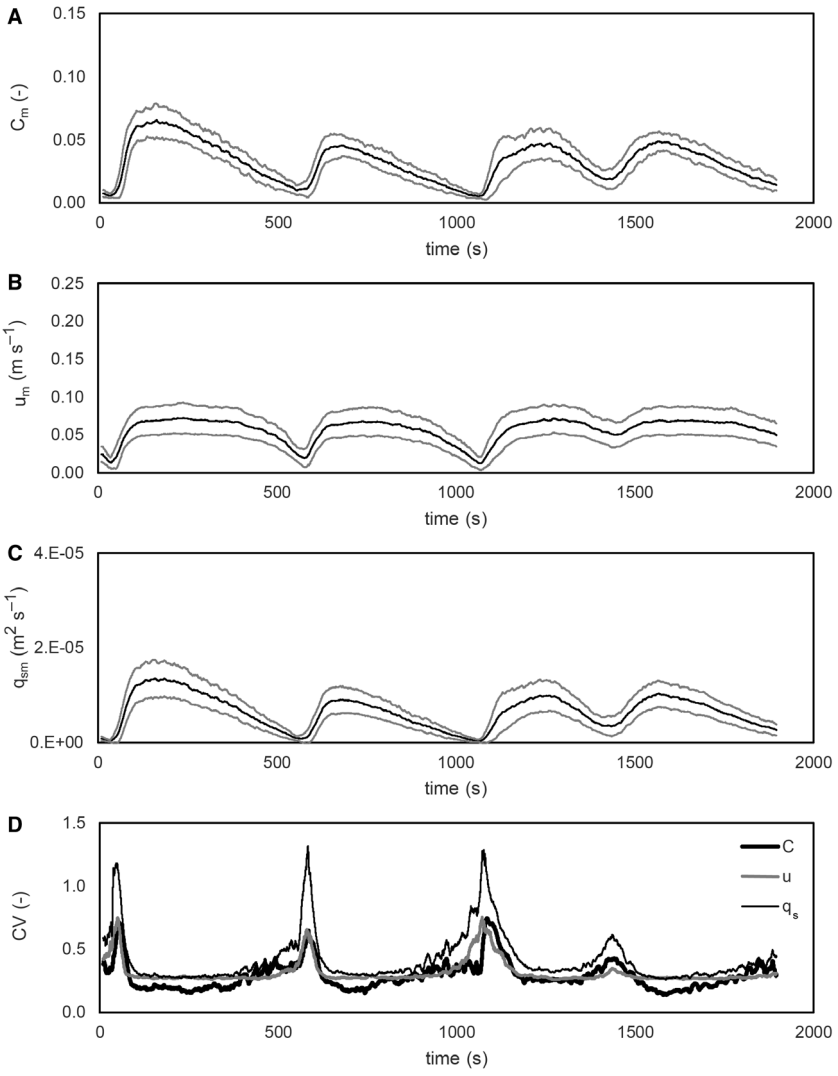

Fig. 9. Mean sediment–kinematics properties on dunes as temporal signals averaged over all the possible realizations (one realization corresponding to one measurement location): (A) concentration of moving sediment, (B) sediment velocity and (C) sediment transport rate at a sample location. (D) Coefficient of variation among the realizations of the quantities. Variation ranges in panels (A) to (C) correspond to one standard deviation.

propagation by means of Cumulative Frequency Distributions (CFD) from data samples. For the dune and gust celerity, the samples are those based on which the average celerity values were provided above. For the sediment velocity, instead, the sample is the temporal signal with 0.26 s moving average presented in Fig. 4 (that is representative of all of the sediment velocity data). The sample sizes are quite different from one another, returning more or less smooth shapes of the distributions. A log axis is used for the celerity values because the latter span two orders of magnitude (the use of a log axis is also the obvious reason for not displaying the left tail of the distribution for the sediment velocity). The distribution for the sediment gusts was not fully resolved, probably because the sampling frequency of the experimental movie was not sufficient for that purpose. However, Fig. 10 supports a cascade where the different scales of propagation can be related to sediment or water waves or to the velocity of the sediment particles.

It should be mentioned that the scale separation demonstrated in the plot of Fig. 10 is somehow determined by the choice of the features whose propagation was investigated (for example, the presence of smaller bedforms superimposed to the main dunes – e.g. Venditti & Church, 2005 – was neglected or filtered out by long-term averaging), while the sediment transport in bed-load dunes is rather a process with a continuous spectrum (e.g. Nikora *et al.*, 1997; Singh *et al.*, 2011; Guala *et al.*, 2014). A frequency spectrum for a time signal of concentration is depicted in Fig. 11, starting from the

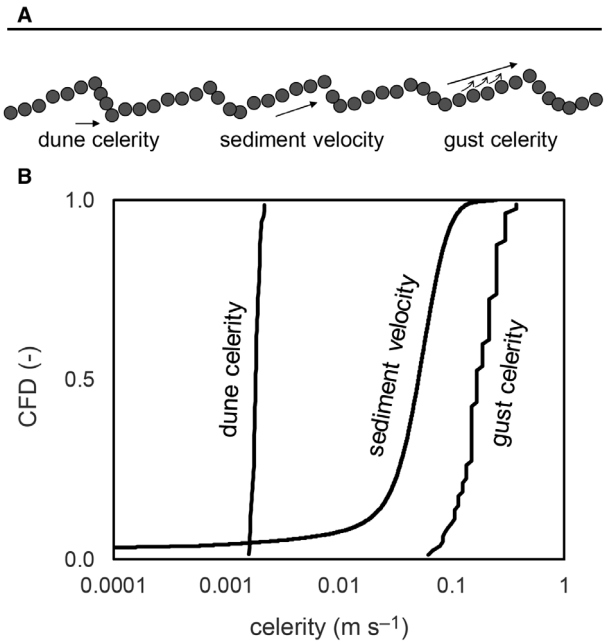

Fig. 10. Multi-scale propagation in bed-load dunes: (A) conceptual picture, where the upper line corresponds to the flume lid and the celerity of individual features is sketched only once; (B) experimental evidence by Cumulative Frequency Distributions of the measured celerity of bed-load dunes, sediment velocity and celerity of sediment gusts.

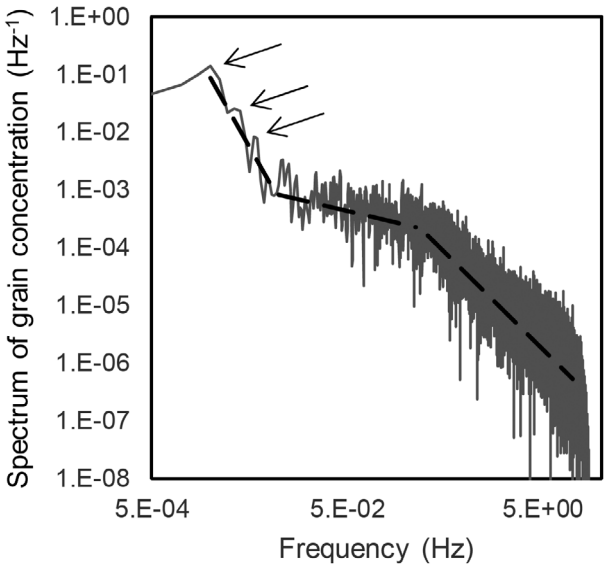

Fig. 11. Frequency spectrum (with major peaks highlighted) of the concentration signal depicted in Fig. 4 (without any regularization by moving average). The dashed lines are for scaling slopes of −3, −2/5 and −5/3 (from the lowest to the highest frequencies).

time history of Fig. 4 (but without any moving average). Major peaks in power spectral density are obtained for frequencies of 0.002 Hz, 0.004 Hz and 0.006 Hz. The first one is consistent with four dunes being present in a time history of around 2000 s and is thus related to the period of the dunes. The others are also low-frequency peaks, and might be related to the periods of smaller bedforms superimposed onto the dunes. The fluctuations related to the flow turbulence are instead much less energetic. For frequencies in a range approximately between 0.001 Hz and 0.01 Hz, the spectrum has a slope of around −3, consistent with those for measurements of bed elevation (Nikora *et al.*, 1997; Coleman & Nikora, 2011; Radice, 2019). This frequency range is also in reasonable agreement with that of the runs with sand of Singh *et al.* (2011), who however reported a slope of −2.5. After a transition with a much lower slope, in a range approximately between 0.3 Hz and 10 Hz the slope is around −5/3, consistent with that of a turbulence spectrum as reported by Radice *et al.* (2009, 2010) for an experiment with weak bed-load transport over a plane bed.

The separation between the dune celerity and the sediment velocity requires a precise definition of which sediment velocity is being considered or, in other words, of the particles with reference to which velocity is measured. The velocity of the surface sediment, measured in a Eulerian manner in this work, is larger than the dune celerity, but the particles are not always the same as different bed-load particles lie on the bed surface at different times. If one instead considers the Lagrangian velocity of one particle, its relationship to the dune celerity will depend on the scale of analysis. In the short-term, particles over the dune tails perform bed-load hops (e.g. Ashley *et al.*, 2020), with velocities that may be similar to those measured in this study for the same locations. In the long-term, instead, one can expect that the sediment velocity and the dune celerity will be equal to one another, as clarified by a simple concept. Consider a bed-load particle that: (i) travels along the dune with a constant velocity u (in this simplifying scheme the hops are neglected); then (ii) passes the dune front and gets buried just downstream of it; (iii) remains buried for one dune period; and finally (iv) restarts the cycle. The distance travelled by the particle is the dune length L; the time taken to travel the dune is L/u, but the particle then remains still

for a time equal to T, that is the dune period, also equal to the time needed for next particle exhumation. Then, the velocity of the particle is:

$$u_v = \frac{L}{(L/u)+T} \cong \frac{L}{T} = c \tag{2}$$

with c as the dune celerity of propagation. The long-term particle velocity is indicated as u_v, meaning a 'virtual' particle velocity as used in several studies of particle tracking in the field (e.g. Mao *et al.*, 2016; Ferguson *et al.*, 2017; Ivanov *et al.*, 2020), where the scale of observation cannot be as fine as in the laboratory.

Mean sediment–kinematics patterns

The scale separation discussed above was used to support a Taylor-like hypothesis, in order to find mean sediment–kinematics patterns over a train of dunes, and to convert a temporal signal into a spatial profile. This assumption should be viewed as a first-order approximation, since it is known that the dunes in a train may have different propagation celerity (e.g. Coleman *et al.*, 2003; Guala *et al.*, 2014; Ancey, 2020). As a matter of fact, the signals of Figs 4 and 9 show that a trough between the third and fourth dune did not reach very low values of the kinematic properties, possibly pointing to future coalescence with the fourth dune taking over the third. However, McElroy & Mohrig (2009) introduced a 'deformation flux' related to continuous, zero-mean deformation of a dune-train profile; they also presented an estimation of such flux for a laboratory experiment showing that, in laboratory conditions, the deformation flux was negligible compared to the total flux. Based on this assessment, it can be reasonably assumed that the construction of a mean sediment motion pattern done in this work is sufficiently reliable. A Taylor-like hypothesis may instead fail in cases with larger dune deformation.

The data presented in this manuscript are quite rich compared with analogous examples in the literature. To the best of the authors' knowledge, the data available in the literature for image-based measurement of sediment transport in bed-load dunes are those of Tsubaki *et al.* (2018) and Terwisscha van Scheltinga *et al.* (2018, 2019), that were already mentioned above. The added value of the present study compared to those prior ones lies in the consideration of the sediment concentration that enabled a sediment transport rate to be computed, and in the long duration that enabled a statistical stability of the mean sediment flux to be achieved after four full dunes. Furthermore, large spatial domains may be beneficial when analyzing morphological processes (e.g. Redolfi *et al.*, 2017). In the present work the area of investigation was not very long in the streamwise direction, and the presence of multiple measurement cells was actually used to produce realizations of a temporal signal for averaging, rather than showing spatial distributions. However, the successive conversion from the temporal to the spatial domain allowed a depiction of a dune profile along more than 3 m.

Impact of the present findings

The above *Results* and *Discussion* provide significant phenomenological insight into bed-load dunes for the applied flow condition, answering the key question posed in the *Introduction*. The present sub-section answers a further question: 'what is the usefulness of these results?', with reference to three issues.

First, the present results fill an existing gap because previous research on sediment kinematics for subaqueous bed-load dunes has mostly considered the sediment velocity without a systematic consideration of the sediment concentration (Terwisscha van Scheltinga *et al.*, 2018, 2019; Tsubaki *et al.*, 2018). On the other hand, sediment transport fluxes are related to both concentration and velocity of transported particles. Thus, formulations of the bed-load transport rate involving the concentration of moving sediment may benefit from the present results that include long-duration time evolutions of sediment concentration, velocity and transport rate along four full dunes. The measurements presented in this manuscript also enabled the correlations between the properties to be quantitatively assessed, and the computation of mean sediment motion for the investigated portion of a dune train. Further work may shed light on how the sediment motion over a dune reacts to spatial changes in bed elevation and, in turn, near-bed flow velocity and shear stress.

Second, field monitoring of sediment transport sometimes involves the measurement of surrogate quantities that can be later converted into a sediment transport rate by a calibrated transfer function. The typical case is that of measuring an apparent velocity of the bed with acoustic instruments and converting this

velocity into a sediment transport rate (see, for example, Rennie & Millar, 2004; Gaeuman & Jacobson, 2006; Conevski *et al.*, 2019). A multi-scale propagation, like the one demonstrated in this manuscript, thus requires an appropriate assessment of the sediment velocity under consideration and of its link to the sediment transport rate.

Finally, quantitative results on dune propagation and associated sediment transport rates are crucial in scour research under the so-called live-bed conditions, because generalized sediment transport and dune migration are the background for these local processes. A general description of live-bed scour processes is that a measured scour depth fluctuates in time as a result of the fluctuations of the sediment transport rate into the scour hole. However, for a detailed investigation of the link between the two fluctuation patterns, a time record of dune-induced sediment transport rate is essential. In the absence of this, one has to use simplified models for the oscillations. For example, Hong *et al.* (2017) presented a mathematical model of the scour process at a bridge pier and, lacking a typical time series of sediment discharge from the upstream reach, used a sinusoidal function for the incoming sediment transport rate. The present results instead demonstrate that the sediment transport flux for a dune train is not sinusoidal; using a sediment flux signal as measured in this study would make mathematical models of the live-bed scour process much more similar to reality.

CONCLUSIONS

This study presented a long-duration laboratory experiment where the kinematics of bed-load grains were measured by image processing over a succession of dunes. The observation of the sediment motion over the dune surface revealed phenomenological properties that go much beyond what can be observed by bed scanning, and are thus important for process investigation and validation of theories. On the other hand, a detailed investigation of the sediment kinematics is demanding and unavoidably hinders the possibility to perform extensive experimental campaigns with a variety of hydro-dynamic conditions (this remaining a challenge for future research).

In the present investigation, a sequence of four dunes was sufficient to obtain a statistical stability of the mean values for sediment–kinematics properties at a single measuring location (the analysis of the stability of mean values is needed because all of the investigated properties – sediment concentration, velocity and transport rate – fluctuate in time). The temporal evolution of the sediment transport was similar in shape to that of the concentration of moving particles, while the sediment velocity presented a different, and smoother, fluctuation pattern. Fluctuations occurred at a wide spectrum of scales; a multi-feature, multi-scale propagation dynamics was demonstrated by observing how the temporal signals for neighbouring locations were offset in time.

In the presence of a wide range of propagation scales, the lowest one (the celerity of the dunes) could be used in a Taylor-like hypothesis to determine a mean sediment motion pattern over a dune train. The Taylor-like hypothesis must be viewed as a first-order approximation while, in more detail, the different parts of the dune train may propagate at different celerities.

The results of this investigation are relevant for a variety of studies and applications, ranging from detailed investigations of dune dynamics to applications where the time evolution of the sediment motion over a dune train represents a boundary condition for the investigation of another process (for example, local sediment erosion at a key spot).

ACKNOWLEDGEMENTS

The first version of this manuscript was written during a lockdown imposed in Italy after the spread of COVID-19. It was kind of strange to prepare this while many people were working hard to face the emergency; we are obliged to these highly-committed people. I gratefully acknowledge Francesco Ballio for stimulating the laboratory experiment, and Thomas Cannella, Giacomo Inzaghi and Mattia Pullano for contributing to this research during their B. Sc. theses. Arnoud Slootman and an anonymous reviewer provided insightful comments that enabled the manuscript to be improved.

DATA AVAILABILITY STATEMENT

The movie of the experiment is available upon request.

REFERENCES

Ancey, C. (2020) Bedload transport: a walk between randomness and determinism. Part 1. The state of the art. *J. Hydraul. Res.*, **58**, 1–17. https://doi.org/10.1080/00221686.2019.1702594.

Ancey, C., **Davison, A.C.**, **Böhm, T.**, **Jodeau, M.** and **Frey, P.** (2008) Entrainment and motion of coarse particles in a shallow water stream down a steep slope. *J. Fluid Mech.*, **595**, 83–114. https://doi.org/10.1017/S0022112007008774.

Ashley, T.C., **Mahon, R.C.**, **Naqshband, S.**, **Leary, K.C.P.** and **McElroy, B.** (2020) Probability distributions of particle hop distance and travel time over equilibrium mobile bedforms. *J. Geophys. Res. Earch Surf.*, **125**, https://doi.org/10.1029/2020JF005647.

Ballio, F. and **Guadagnini, A.** (2004) Convergence assessment of numerical Monte Carlo simulations in groundwater hydrology. *Water Resour. Res.*, **40**, W04603. https://doi.org/10.1029/2003WR002876.

Ballio, F., **Pokrajac, D.**, **Radice, A.** and **Hosseini Sadabadi, S.A.** (2018) Lagrangian and Eulerian description of bed load transport. *J. Geophys. Res. Earch Surf.*, **123**, 384–408. https://doi.org/10.1002/2016JF004087.

Best, J. (2005) The fluid dynamics of river dunes: a review and some future research directions. *J. Geophys. Res. Earch Surf.*, **110**, F04S02. https://doi.org/10.1029/2004JF000218.

Buffington, J.M. (1999) The legend of A. F. Shields. *J. Hydraul. Eng.*, **125**, 376–387. https://doi.org/10.1061/(ASCE)0733-9429(1999)125:4(376).

Buffington, J.M. and **Montgomery, D.R.** (1997) A systematic analysis of eight decades of incipient motion studies, with special reference to gravel-bedded rivers. *Water Resour. Res.*, **33**, 1993–2029. https://doi.org/10.1029/96WR03190.

Campagnol, J., **Radice, A.**, **Nokes, R.**, **Bulankina, V.**, **Lescova, A.** and **Ballio, F.** (2013) Lagrangian analysis of bed-load sediment motion: database contribution. *J. Hydraul. Res.*, **51**, 589–596. https://doi.org/10.1080/00221686.2013.812152.

Campagnol, J., **Radice, A.**, **Ballio, F.** and **Nikora, V.** (2015) Particle motion and diffusion at weak bed load: accounting for unsteadiness effects of entrainment and disentrainment. *J. Hydraul. Res.*, **53**, 633–648. https://doi.org/10.1080/00221686.2015.1085920.

Cardona Florez, J.E. and **De Moraes Franklin, E.** (2016) The formation and migration of sand ripples in closed conduits: experiments with turbulent water flows. *Exp. Thermal. Fluid Sci.*, **71**, 95–102. https://doi.org/10.1016/j.expthermflusci.2015.10.017.

Charru, F., **Andreotti, B.** and **Claudin, P.** (2013) Sand ripples and dunes. *Annu. Rev. Fluid Mech.*, **45**, 469–493. https://doi.org/10.1146/annurev-fluid-011212-140806.

Coleman, S.E., **Fedele, J.J.** and **Garcia, M.H.** (2003) Closed-conduit bed-form initiation and development. *J. Hydraul. Eng.*, **129**(12), 956–965. https://doi.org/10.1061/(ASCE)0733-9429(2003)129:12(956).

Coleman, S.E. and **Nikora, V.I.** (2011) Fluvial dunes: initiation, characterization, flow structure. *Earth Surf. Proc. Land.*, **36**, 39–57. https://doi.org/10.1002/esp.2096.

Conevski, S., **Guerrero, M.**, **Ruther, N.** and **Rennie, C.D.** (2019) Laboratory investigation of apparent bedload velocity measured by ADCPs under different transport conditions. *J. Hydraul. Eng.*, **145**(11), 956–965. https://doi.org/10.1061/(ASCE)HY.1943-7900.0001632.

Drake, T.G., **Shreve, R.L.**, **Dietrich, W.E.**, **Whiting, P.J.** and **Leopold, L.B.** (1988) Bedload transport of fine gravel observed by motion-picture photography. *J. Fluid Mech.*, **192**, 193–217. https://doi.org/10.1017/S0022112088001831.

Engelund, F. and **Fredsøe, J.** (1982) Sediment ripples and dunes. *Annu. Rev. Fluid Mech.*, **14**, 13–37. https://doi.org/10.1146/annurev.fl.14.010182.000305.

Fathel, S.L., **Furbish, D.J.** and **Schmeeckle, M.W.** (2015) Experimental evidence of statistical ensemble behavior in bed load sediment transport. *J. Geophys. Res. Earch Surf.*, **120**, 2298–2317. https://doi.org/10.1002/2015JF003552.

Ferguson, R.I., **Sharma, B.P.**, **Hodge, R.A.**, **Hardy, R.J.** and **Warburton, J.** (2017) Bed load tracer mobility in a mixed bedrock/alluvial channel. *J. Geophys. Res. Earch Surf.*, **122**, 807–822. https://doi.org/10.1002/2016JF003946.

Fraccarollo, L. and **Hassan, M.A.** (2019) Einstein conjecture and resting-time statistics in the bed-load transport of monodispersed particles. *J. Fluid Mech.*, **876**, 1077–1089. https://doi.org/10.1014/jfm.2019.563.

Frey, P., **Ducottet, C.** and **Jay, J.** (2003) Fluctuations of bed load solid discharge and grain size distribution on steep slopes with image analysis. *Exp. Fluids*, **35**, 589–597. https://doi.org/10.1007/s00348-003-0707-9.

Furbish, D.J., **Fathel, S.L.**, **Schmeeckle, M.W.**, **Jerolmack, D.J.** and **Schumer, R.** (2017) The elements and richness of particle diffusion during sediment transport at small timescales. *Earth Surf. Proc. Land.*, **42**, 214–237. https://doi.org/10.1002/esp.4084

Gaeuman, D. and **Jacobson, R.B.** (2006) Acoustic bed velocity and bed load dynamics in a large sand bed river. *J Geophys. Res. Earth Surf.*, **111**(F2), 1–14. https://doi.org/10.1029/2005JF000411

Guala, M., **Singh, A.**, **BadHeartBull, N.** and **Foufoula-Georgiou, E.** (2014) Spectral description of migrating bed forms and sediment transport. *J. Geophys. Res. Earch Surf.*, **119**, 123–137. https://doi.org/10.1002/2013JF002759.

Heays, K.G., **Friedrich, H.**, **Melville, B.W.** and **Nokes, R.** (2014) Quantifying the dynamic evolution of graded gravel beds using particle tracking velocimetry. *J. Hydraul. Eng.*, **140**(7), 04014027. https://doi.org/10.1061/(ASCE)HY.1943-7900.0000850.

Heyman, J., **Bohorquez, P.** and **Ancey, C.** (2016) Entrainment, motion and deposition of coarse particles transported by water over a sloping mobile bed. *J. Geophys. Res. Earch Surf.*, **121**, 1931–1952. https://doi.org/10.1002/2015JF003672.

Hong, J.H., **Chiew, Y.M.**, **Yeh, P.H.** and **Chan, H.C.** (2017) Evolution of local pier-scour depth with dune migration in subcritical flow conditions. *J. Hydraul. Eng.*, **143**(4), 04016098. https://doi.org/10.1061/(ASCE)HY.1943-7900.001261.

Ivanov, V., **Radice, A.**, **Papini, M.** and **Longoni, L.** (2020) Event-scale pebble mobility observed by RFID tracking in a pre-Alpine stream: a field laboratory. *Earth Surf. Proc. Land.*, **45**, 535–547. https://doi.org/10.1002/esp.4752.

Jackson, R.G. (1976) Sedimentological and fluid-dynamic implications of the turbulent bursting phenomenon in geophysical flows. *J. Fluid Mech.*, **77**, 531–560. https://doi.org/10.1017/S0022112076002243.

Julien, P.Y. and **Klaassen, G.J.** (1995) Sand-dune geometry of large rivers during floods. *J. Hydraul. Eng.*, **121**(9), 657–663. https://doi.org/10.1061/(ASCE)0733-9429(1995)121:9(657).

Kadota, A. and **Nezu, I.** (1999) Three-dimensional structure of space-time correlation on coherent vortices generated

behind dune crest. *J. Hydraul. Res.*, **37**(1), 59–80. https://doi.org/10.1080/00221689909498532.

Kuhnle, R.A., **Horton, J.K.**, **Bennett, S.J.** and **Best, J.L.** (2006) Bedforms in bimodal sand-gravel sediments: laboratory and field analysis. *Sedimentology*, **53**, 631–654. https://doi.org/10.1111/j.1365-3091.2005.00765.x.

Lajeunesse, E., **Malverti, L.** and **Charru, F.** (2010) Bed load transport in turbulent flow at the grain scale: experiments and modeling. *J. Geophys. Res. Earch Surf.*, **115**, F04001. https://doi.org/10.1029/2009JF001628.

Mao, L., **Picco, L.**, **Lenzi, M.A.** and **Surian, N.** (2016) Bed material transport estimate in large gravel-bed rivers using the virtual velocity approach. *Earth Surf. Proc. Land.*, **42**, 595–611. https://doi.org/10.1002/esp.4000.

McElroy, B. and **Mohrig, D.** (2009) Nature of deformation of sandy bed forms. *J. Geophys. Res. Earth Surf.*, **114**, F00A04. https://doi.org/10.1029/2008JF001220.

Nelson, J.M. and **Smith, J.D.** (1989) Mechanics of flow over ripples and dunes. *J. Geophys. Res. Oceans*, **94**(C6), 8146–8162. https://doi.org/10.1029/JC094iC06p08146.

Nikora, V.I., **Sukhodolov, A.N.** and **Rowinski, P.M.** (1997) Statistical sand wave dynamics in one-directional water flows. *J. Fluid Mech.*, **351**, 17–39. https://doi.org/10.1017/S0022112097006708.

Radice, A. (2009) Use of the Lorenz curve to quantify statistical nonuniformity of sediment transport rate. *J. Hydraul. Eng.*, **135**(4), 320–326. https://doi.org/10.1061/(ASCE)0733-9429(2009)135:4(320).

Radice, A. (2019) *Experimental characterization of bed-load dunes in a closed conduit: size, period, and migration celerity. Proceedings of the XXXVIII Congress of IAHR*, Panama City, Panama.

Radice, A. and **Ballio, F.** (2008) Double-average characteristics of sediment m(otion in one-dimensional bed load. *Acta Geophys.*, **56**(3), 654–668. https://doi.org/10.2478/s11600-008-0015-0.

Radice, A., **Ballio, F.** and **Nikora, V.** (2009) On statistical properties of bed load sediment concentration. *Water Resour. Res.*, **45**, W06501. https://doi.org/10.1029/2008WR007192.

Radice, A., **Ballio, F.** and **Nikora, V.** (2010) Statistics and characteristic scales for bed load in a channel flow with sidewall effects. *Acta Geophys.*, **58**(6), 1072–1093. https://doi.org/10.2478/s11600-010-0020-y.

Radice, A. and **Lauva, O.** (2017) Live-bed pier scour in a covered flow. *J. Hydraul. Eng.*, **143**(10), 06017016. https://doi.org/10.1061/(ASCE)HY.1943-7900.0001359.

Radice, A., **Malavasi, S.** and **Ballio, F.** (2006) Solid transport measurements through image processing. *Exp. Fluids*, **41**, 721–734. https://doi.org/10.1007/s00348-006-0195-9.

Radice, A., **Nikora, V.**, **Campagnol, J.** and **Ballio, F.** (2013) Active interactions between turbulence and bed load: conceptual picture and experimental evidence. *Water Resour. Res.*, **49**(1), 90–99. https://doi.org/10.1029/2012WR012255.

Radice, A., **Sarkar, S.** and **Ballio, F.** (2017) Image-based Lagrangian particle tracking in bed-load experiments. *J. Visual. Exp.*, **125**, e55874. https://doi.org/10.3791/55874.

Redolfi, M., **Guidorizzi, L.**, **Tubino, M.** and **Bertoldi, W.** (2017) Capturing the spatiotemporal variability of bedload transport: a time-lapse imagery technique. *Earth Surf. Proc. Land.*, **42**, 1140–1147. https://doi.org/10.1002/esp.4126.

Rennie, C.D. and **Millar, R.G.** (2004) Measurement of the spatial distribution of fluvial bedload transport velocity in both sand and gravel. *Earth Surf. Proc. Land.*, **29**(10), 1173–1193. https://doi.org/10.1002/esp.1074.

Van Rijn, L.C. (1984) Sediment transport, part III: bed forms and alluvial roughness. *J. Hydraul. Eng.*, **110**(12), 1733–1754. https://doi.org/10.1061/(ASCE)0733-9429(1984)110:12(1733).

Roseberry, J.C., **Schmeeckle, M.W.** and **Furbish, D.J.** (2012) A probabilistic description of the bed load sediment flux: 2. Particle activity and motions. *J. Geophys. Res. Earch Surf.*, **117**, F03032. https://doi.org/10.1029/2012JF002353.

Schvidchenko, A.B. and **Pender, G.** (2000) Initial motion of streambeds composed of uniform sediments. *Proc. Inst. Civil Eng. Water Maritime Energy*, **142**(4), 217–227. https://doi.org/10.1680/wame.2000.142.4.217.

Singh, A., **Lanzoni, S.**, **Wilcock, P.R.** and **Foufloula-Georgiou, E.** (2011) Multiscale statistical characterization of migrating bed forms in gravel and sand bed rivers. *Water Resour. Res.*, **47**, W12526. https://doi.org/10.1029/2010WR010122.

Taylor, G.I. (1398) The spectrum of turbulence. *Proc. Roy. Soc. London*, **164**, 476–490.

Terwisscha van Scheltinga, R.C., **Coco, G.** and **Friedrich, H.** (2019) Sand particle velocities over a subaqueous dune slope using high-frequency image capturing. *Earth Surf. Proc. Land.*, **44**, 1881–1894. https://doi.org/10.1002/esp.4617.

Terwisscha van Scheltinga, R.C., **Friedrich, H.** and **Coco, G.** (2018) A PIV-based method to measure spatial gradients in bedload transport over a dune. *E3S Web of Conferen.*, **40**, 04012. https://doi.org/10.1051/e3sconf/20184004012

Tsubaki, R., **Baranya, S.**, **Muste, M.** and **Toda, Y.** (2018) Spatio-temporal patterns of sediment particle movement on 2D and 3D bedforms. *Exp. Fluids*, **59**, 93. https://doi.org/10.1007/s00348-018-2551-y.

Unsworth, C.A., **Parsons, D.R.**, **Hardy, R.J.**, **Reesink, A.J.H.**, **Best, J.L.**, **Ashworth, P.J.** and **Keevil, G.M.** (2018) The impact of nonequilibrium flow on the structure of turbulence over river dunes. *Water Resour. Res.*, **54**, 6566–6584. https://doi.org/10.1029/2017WR021377.

Venditti, J.G., **Church, M.** and **Bennett, S.J.** (2005) Morphodynamics of small-scale superimposed sand waves over migrating dune bed forms. *Water Resour. Res.*, **41**, W10423. https://doi.org/10.1029/2004WR003461.

Venditti, J.G., **Martin Lin, C.Y.** and **Kazemi, M.** (2016) Variability in bedform morphology and kinematics with transport stage. *Sedimentology*, **63**, 1017–1039. https://doi.org/10.1111/sed.12247.

Wenzel, J.L. and **De Moraes Franklin, E.** (2019) Velocity fields and particle trajectories for bed load over subaqueous barchan dunes. *Granular Matter*, **21**(3), 75. https://doi.org/10.1007/s10035-019-0928-0.

Wilson, G.W. and **Hay, A.E.** (2016) Acoustic observations of near-bed sediment concentration and flux statistics above migrating sand dunes. *Geophys Res Lett*, **43**, 6304–6312. https://doi.org/10.1002/2016GL069579.

Manuscript received 23 February 2021; revision accepted 27 May 2021

Supporting Information

Additional information may be found in the online version of this article:

File S1. This is a short video representative of the experiment (with image size and sampling rate reduced).

File S2. This is a video that corresponds to File S1 but was produced with images created as differences between successive frames, to highlight the moving sediment.

File S3. This is a screen-capture video that demonstrates the procedure followed to obtain Fig. 3.

File S4. This file presents a few plots that were not included in the manuscript to save some space: plots like those of Fig. 4 with a logarithmic time axis and plots like those of Fig. 9 but with a conversion to a spatial profile.